Supplement of The Cryosphere, 19, 3227–3251, 2025
https://doi.org/10.5194/tc-19-3227-2025-supplement

The Cryosphere Open Access EGU

Supplement of

Modeling mixing and melting in laminar seawater intrusions under grounded ice

Madeline S. Mamer et al.

Correspondence to: Madeline S. Mamer (mmamer3@gatech.edu)

This supplementary document provides additional data and analyses to compliment the findings in the main publication. Here, we present additional vertical profiles for varying turbulence levels, to illustrate the negligible role of mixing in shaping water column structure for the flow environments tested here. We also provide density transects from additional test cases beyond those discussed in the main text for the simulations with varied subglacial environment geometry. Temperature-salinity (TS) diagrams are included to highlight water mass characteristics amongst the freshwater velocities tested as well as between non-melting and melting cases.

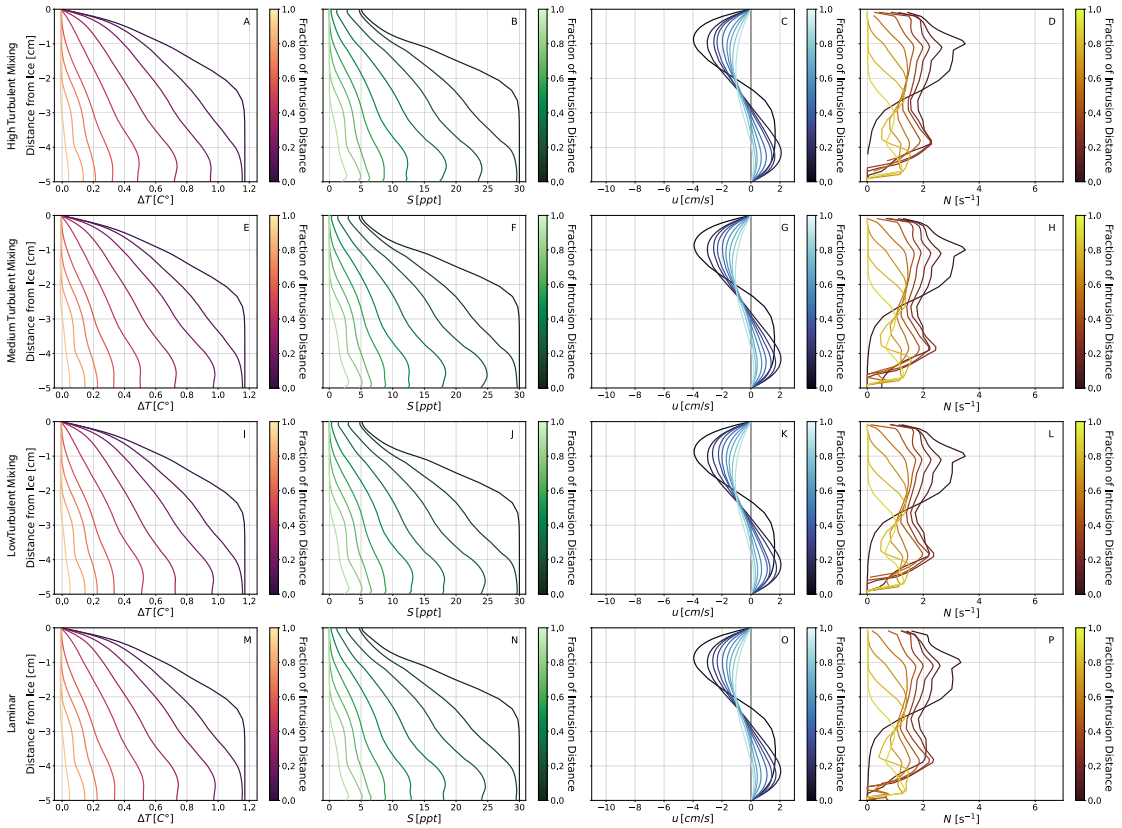

Figure S1. Time-averaged vertical profiles of thermal forcing (A, E, I, M), salinity (B, F, J, N), x-direction velocity (C, G, K, O), and buoyancy frequency (D, H, L, P) for u_f = 0.5 cm s^{-1} across all turbulence levels tested in this study. The top row (A-D) is for C_μ = 0.18, the second row is for C_μ = 0.09, the third row is for C_μ = 0.045, and the bottom row is for no turbulent mixing (aka laminar flow). Each line is colored by is respective "fraction of intrusion distance", i.e. where its location is relative to the intrusion distance. Darker lines represent closer to the grounding line, where the intrusion would be at its thickest point. Lighter lines represent further upstream near the head of the intrusion.

Turbulent mixing has little to no role in setting seawater intrusion distance or vertical dynamics (Figure S1). There is essentially no change in the vertical structure of the intrusion between the highest degree of mixing (Figure S1A-D) and the lowest degree of mixing (Figure S1M-P). This is because the flows simulated in this study have low Reynolds numbers. Therefore the flows have a low turbulent viscosity of the same magnitude as the kinematic viscosity of seawater. This points to viscous processes dominating this subcritical subglacial discharge regime, which allows seawater to intrude.

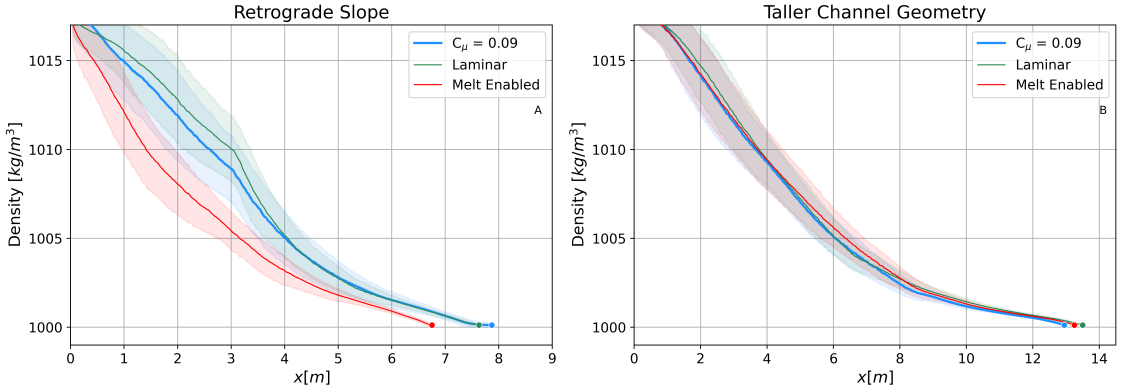

Figure S2. Depth-averaged transects of density within the subglacial environment from the time-average of the quasi-steady-state results. Panel A is for u_f = 0.5 cm s^{-1} with a retrograde bed slope where $\Theta = 0.5°$. Panel B is for the same u_f, but with a flat bed and taller subglacial environment (H = 7.5 cm). The blue transects represent simulations with medium turbulent mixing and are the same as the orange and pink lines in Figure 2 from the main text. The green transects represent the intrusions for the laminar simulations, and the red transects represent the intrusion for melt-enabled simulations. The dots represent the total intrusion distance for their respective case.

In addition to testing the alternate geometries with standard turbulent mixing for u_f = 0.5 cm s^{-1}, we also simulated them with laminar flow and a melt-enabled boundary. For the retrograde geometry, there is little difference in the intrusion distance between the laminar flow case and the medium turbulent mixing case, however, the intrusion distance is reduced when melting is enabled (Figure S2A). For the taller geometry, little change happens in intrusion distance when either turbulent mixing is turned off or melting is enabled (Figure S2B).

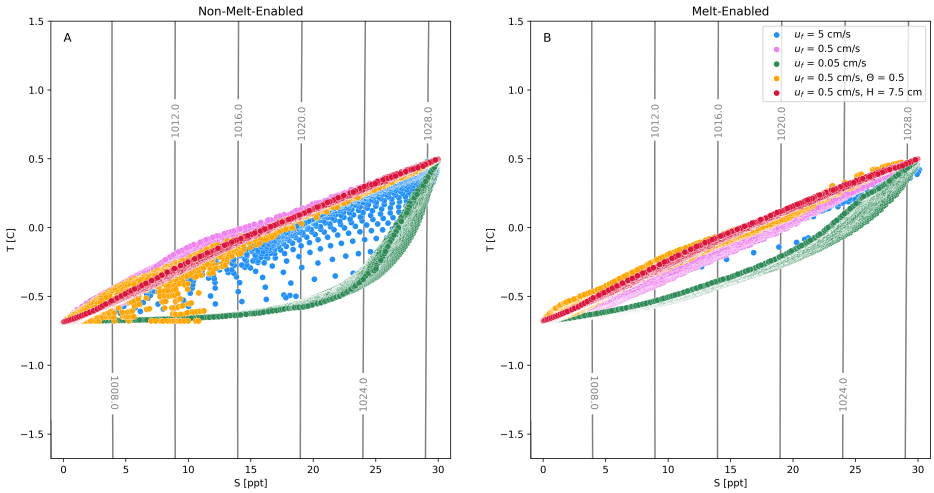

Figure S3. Temperature and Salinity diagram for the non-melt enabled simulations with medium turbulent mixing (C_μ = 0.09). The points only represent the domain within the seawater intrusion for that respective case. The data for this figure comes from the time-averaged domain from the quasi-steady-state period. Note, that there are a lot more data points than what is shown, but to help with readability we limited the data shown.

The temperature and salinity within the intrusion were plotted on a T-S diagram for each freshwater velocity and geometry tested in both melting and non-melting simulations (Figure S3A and Figure S3B). In most simulations, the mixing follows a straight line between the freshwater and seawater water masses. However, in the case with the slowest freshwater velocity, the mixing line exhibits a "bend," which may suggest additional mixing processes or the formation of another water mass within the intrusion.

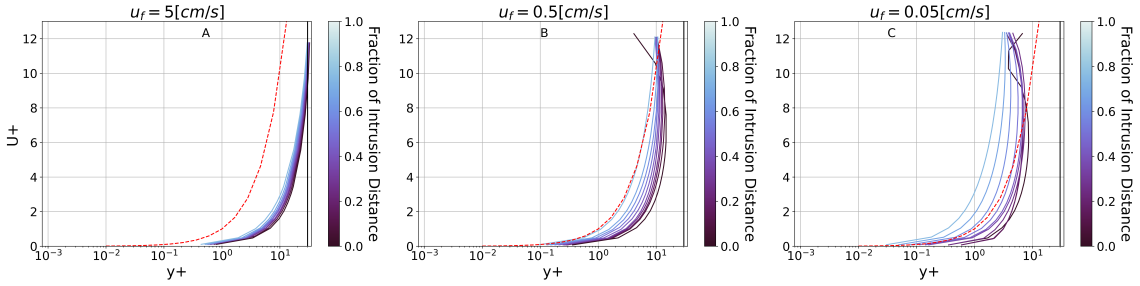

Figure S4. Law of the wall figure for each freshwater velocity with standard geometry (flat bottom, H = 5 cm) and medium turbulent mixing (C_μ = 0.09). The non-dimensionalized distance from the wall is on the x-axis, and the non-dimensionalized velocity is on the y-axis. As y+ approaches 0, the fluid is near the ice. The black line represents y+ = 30, which is where the freestream should begin. The red dashed line represents where U+ = y+ and denotes the region of the viscous boundary layer. Each line represents a profile along the intrusion at evenly placed intervals.

The structure of a boundary layer can be visualized by non-dimensionalizing the distance from the boundary and the streamwise velocity of the fluid. The velocity is non-dimensionalized by dividing it by the squared shear velocity. The distance from the wall is non-dimensionalized by dividing it by the kinematic viscosity and multiplying it by the shear velocity. These values typically exhibit a logarithmic relationship starting near the edge of the boundary layer and extending outward into the freestream flow, which usually occurs around y+ $\sim$ 30 (Pope, 2000). The relationship is linear within the boundary layer (y+ < 30) (Pope, 2000). This characteristic can be used to assess whether a boundary layer fully develops in our simulations of seawater intrusion. However, as shown in Figure S4, the logarithmic portion of this relationship—indicative of flow outside the boundary layer—is absent for all tested freshwater velocities in this simulation.

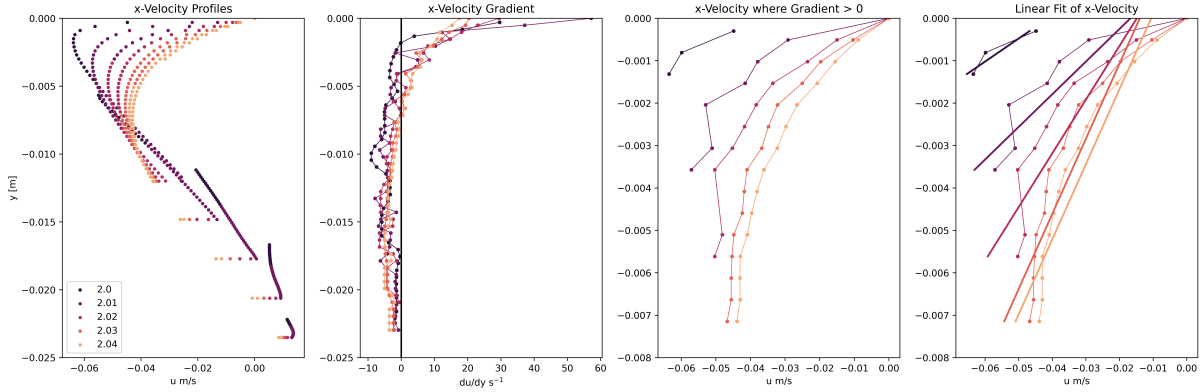

Figure S5. Depicted here is the methodology used to obtain the gradient in velocity near the ice, which exists at y = 0. The first panel depicts profiles of x-direction velocity from the time-averaged solution domain. The second panel is the gradient of this velocity, with respect to y. We then isolate the x-velocity data to where the gradient is positive. This isolation is shown in the third panel. The final panel is this selectively chosen x-direction velocity and the linear fit corresponding to each profile. We use the slope of this linear fit in our calculation for the drag coefficient.

30 To calculate the drag coefficient presented in the main text, we applied a linear fit to the upper half of the freshwater layer's velocity near the ice. The fit was constrained to the region where the local velocity gradient was positive. This methodology, demonstrated for u_f = 0.5 cm s^{-1} with the standard geometry, is shown in Figure S5.

References

Pope, S. B.: Turbulent Flows, Cambridge University Press, Cambridge, UK, https://doi.org/10.1017/CBO9780511840531, 2000.